Molecular Cell
Article

Nuclear Import Mechanism of the EJC Component Mago-Y14 Revealed by Structural Studies of Importin 13

Fulvia Bono,[1,2] Atlanta G. Cook,[1] Marlene Grünwald,[2] Judith Ebert,[1] and Elena Conti[1,*]
[1]Max-Planck-Institute of Biochemistry, Department of Structural Cell Biology, Am Klopferspitz 18, 82152 Martinsried, Germany
[2]Max-Planck-Institute for Developmental Biology, Spemannstrasse 35, 72076 Tübingen, Germany
*Correspondence: conti@biochem.mpg.de
DOI 10.1016/j.molcel.2010.01.007

SUMMARY

Mago and Y14 are core components of the exon junction complex (EJC), an assembly central to nonsense-mediated mRNA decay in humans and mRNA localization in flies. The Mago-Y14 heterodimer shuttles between the nucleus, where it is loaded onto specific mRNAs, and the cytoplasm, where it functions in translational regulation. The heterodimer is imported back into the nucleus by Importin 13 (Imp13), a member of the karyopherin-β family of transport factors. We have elucidated the structural basis of the Mago-Y14 nuclear import cycle. The 3.35 Å structure of the *Drosophila* Imp13-Mago-Y14 complex shows that Imp13 forms a ring-like molecule, reminiscent of Crm1, and encircles the Mago-Y14 cargo with a conserved interaction surface. The 2.8 Å structure of human Imp13 bound to RanGTP reveals how Mago-Y14 is released in the nucleus by a steric hindrance mechanism. Comparison of the two structures suggests how this unusual karyopherin might function in bidirectional nucleocytoplasmic transport.

INTRODUCTION

In eukaryotic cells, the distinct composition of the nucleoplasm is maintained by the selective and directional transport of macromolecules across the nuclear envelope. Nucleocytoplasmic transport occurs via nuclear pore complexes (NPCs) and is mediated, in the vast majority of cases, by the karyopherin-β family of receptors (Cook et al., 2007; Görlich and Kutay, 1999; Terry et al., 2007; Weis, 2003). Nuclear proteins are transported into the nucleus by a subset of karyopherins known as importins, while most classes of RNAs (with the notable exception of messenger RNAs, mRNAs) are transported out of the nucleus by karyopherins known as exportins. Directionality is determined by the RanGTP gradient, created by the presence of high levels of RanGTP in the nucleus and low levels in the cytosol. Importins bind their cargo in the cytosol in the absence of RanGTP and release it in the nucleus upon RanGTP binding. On the contrary, exportins form complexes in the nucleus with RanGTP and their cargo, which is then dissociated upon hydrolysis of GTP to GDP in the cytosol.

While several structural studies to date have revealed the mechanisms by which canonical transport factors mediate unidirectional nuclear import or export (Chook and Blobel, 1999; Cingolani et al., 1999; Cook et al., 2005, 2009; Dong et al., 2009; Lee et al., 2005, 2006; Matsuura and Stewart, 2004; Monecke et al., 2009), it is unclear how other transport factors can support bidirectional mechanisms. Karyopherins such as Importin 13 (Imp13) in metazoans and Msn5 in yeast, for example, have a double functionality in that they can either import or export depending on the specific cargo molecule to which they bind (Mingot et al., 2001; Yoshida and Blobel, 2001). In *Drosophila*, Imp13 is encoded by an essential gene that is required at the neuromuscular junction (Giagtzoglou et al., 2009). In humans, Imp13 has been shown to mediate the nuclear import of cargos, including Mago-Y14 and Ubc9, and to mediate the nuclear export of eIF1A (Mingot et al., 2001).

The import of Mago-Y14 into the nucleus is a prerequisite for its incorporation into messenger ribonucleoprotein particles (mRNPs) that assemble upon splicing (Giorgi and Moore, 2007). As the spliceosome processes intron-containing pre-mRNAs, it loads Mago and Y14 upstream of splice junctions. The loading depends on the presence of the helicase eIF4AIII, and the assembly is then stabilized by a fourth component, Barentsz (Btz, also known as MLN51) (Gehring et al., 2009a; Herold et al., 2009; Zhang and Krainer, 2007). Together, the four proteins form the core of the exon junction complex (EJC), an assembly that endows the mature mRNP with architectural information on the pre-mRNA intron structure long after the introns have been excised (Ballut et al., 2005; Le Hir et al., 2000). The EJC is an integral part of the spliced mRNP and is retained with it during its journey to the cytoplasm. In the cytoplasm, the EJC functions in different aspects of translational control of the mRNP with which it is associated, ranging from nonsense-mediated mRNA decay in human cells to localization of *oskar* mRNA at the posterior pole of *Drosophila* oocytes (Giorgi and Moore, 2007).

After carrying out their cytoplasmic function as part of the EJC, Mago and Y14 are imported back into the nucleus by Imp13 for another round of mRNP incorporation and regulation (Mingot et al., 2001). The dissociation of Mago-Y14 from the EJC requires the action of translating ribosomes on the mRNP as well as the

ribosomally associated protein PYM (Diem et al., 2007; Gehring et al., 2009b). PYM is a cytosolic protein that binds to Mago-Y14, forming a compact ternary complex (Forler et al., 2003; Bono et al., 2004) that is no longer able to interact with eIF4AIII and Barentsz (Chamieh et al., 2008). However, PYM is not imported into the nucleus with Mago-Y14 (Mingot et al., 2001), raising the question of how the Mago-Y14-PYM complex is dissociated prior to nuclear import.

To study the nuclear import mechanism of Mago-Y14, we determined the crystal structures of an Imp13-Mago-Y14 complex and of an Imp13-RanGTP complex, revealing snapshots of both the cytosolic and nuclear steps of the transport cycle. The structures show how the Mago-Y14 heterodimer is specifically recognized and selected away from its interaction with PYM and how the release of Mago-Y14 in the nucleus is achieved. Comparison of the two nuclear import complexes suggests how this unusual karyopherin might function in nuclear export.

RESULTS AND DISCUSSION

Determination of the Structures of Imp13-RanGTP and Imp13-Mago-Y14

To obtain crystals of Imp13 bound to the cargo Mago-Y14 or bound to the regulator RanGTP, we used homologous proteins from different species. This is an established crystallization strategy, based on the rationale that the solvent-exposed molecular surfaces that engage in crystal lattice contacts are often the least-conserved residues in the protein. The three components of the Imp13-Mago-Y14 complex from *H. sapiens* and *D. melanogaster* share 27%, 89%, and 60% sequence identity, respectively (Figures 1 and S1). Orthologs of the GTPase Ran also share about 90% sequence identity from yeast to human (Figure S1). The conservation is such that yeast GTP-bound Ran can interact with Imp13 from either human (see below) or fly (data not shown). Imp13 and Mago-Y14 from *Drosophila* and human can also interact across species in pull-down assays (see below).

Diffracting crystals of Imp13 bound to RanGTP were obtained with a complex composed of full-length *H. sapiens* Imp13 (residues 1–963) and a construct of *S. cerevisiae* Ran encompassing residues 8–179 and containing the Q71L mutation (which impairs the intrinsic GTPase activity of the protein [Bischoff et al., 1994]). The truncations at the N and C termini of Ran (residues 1–219 when full-length) were identified by limited proteolysis (data not shown) and map to the portion of the molecule that is ordered in the crystal structures of other karyopherin complexes (Cook et al., 2007). The 127 kDa binary complex between Imp13 and the nonhydrolytic deletion mutant of Ran (Ran 8–179 Q71L) bound to GTP crystallized in space group $P3_121$, with one molecule per asymmetric unit (ASU). The structure was solved by SAD (single-wavelength anomalous dispersion) phasing with crystals containing selenomethionine (SeMet)-derivatized Imp13. The final model (Figure 2A) has been refined to 2.8 Å resolution with an R_{free} of 26.8%, R_{factor} of 23.6%, and good stereochemistry (data collection and refinement statistics in Table 1). The atomic model consists of Imp13 residues 18–953 (with the exception of residues 153–158, 183–191, and 658–672, which show no ordered electron density) and Ran residues 8–179.

The structure of Imp13 bound to Mago-Y14 (Figure 2B) was obtained by combining full-length *Drosophila* (Dm) Imp13 (residues 1–971) and Mago-Y14 (residues 1–147 and 1–165). The 147 kDa ternary complex crystallized in space group *P*1, with two molecules per ASU. The structure was solved by a combination of molecular replacement and SeMet SAD phasing and has been refined at 3.35 Å resolution to an R_{free} of 28.9% and a R_{factor} of 26.7% (Table 1). The atomic model for Imp13 consists of residues 11–965, with the exception of a number of short inter- and intra-repeat loops that show no ordered electron density. The model of Mago includes residues 3–147, with the exception of residues 42–44 and 106–107 in disordered loops. The model for Y14 spans from residue 67 to 154. The electron density for functionally important regions of the molecules discussed in the text is shown in Figure S2.

Overall Structure of Imp13 in the Cargo-Bound and Ran-Bound Complexes

As with all members of the karyopherin-β family, Imp13 is an all α-helical protein consisting of 20 consecutive helical motifs (Figures 3 and S3). The first 19 are canonical HEAT repeats, each comprising two antiparallel α helices (A and B), while the C-terminal motif (here referred to as HEAT 20) consists of three α helices. The repeats pack side by side in a parallel fashion, generally with a right-handed twist that generates a superhelical molecule with the A helices forming the outer convex surface and the B helices forming the inner concave surface (Figures 3A and 3B, right panels). The loops that connect consecutive repeats (interrepeat) protrude on one side of the molecule, while the loops that connect the A and B helices of each repeat (intrarepeat) protrude on the opposite side (Figures 3A and 3B, left panels). These loops have variable lengths and in several instances contain insertions with small helical segments (Figure 3C). The regular right-handed arrangement of the repeats is interrupted by prominent left-handed turns at HEATs 4 and 10. Other deviations are at the first repeat, which packs with HEAT 2 in an almost perpendicular fashion, and at the last HEAT repeat that caps the superhelix. The packing of the helical repeats in both the Ran and Mago-Y14 complexes is such that the molecule is bent into a toroid shape, although the overall conformation of the karyopherin is different in the two structures (Figure 3).

When in complex with Mago-Y14, Dm Imp13 has a twisted ring-like conformation, with the edge of HEAT 20 approaching the side of HEAT 1 (Figure 3B). The inner surface of the ring measures about 60 Å in diameter, and the outer surface spans about 95 Å in diameter. Mago-Y14 binds at the inner surface of Imp13, shifted toward the side of the ring that features the interrepeat loops (Figures 3B, left panel, and 2B). When bound to RanGTP, human (Hs) Imp13 again has a toroidal conformation, but with a more pronounced twist of the N- and C-terminal repeats with respect to each other (Figure 3A). In the Imp13-RanGTP structure, the edge of HEAT 20 approaches the side of HEAT 4, creating a more compact toroid with an inner diameter of approximately 50–55 Å. Ran occupies half of the inner surface of the ring, shifted toward the protruding N-terminal HEAT repeats (Figures 3A, left panel, and 2A), i.e., toward the opposite side as compared to Mago-Y14. Hs and Dm Imp13

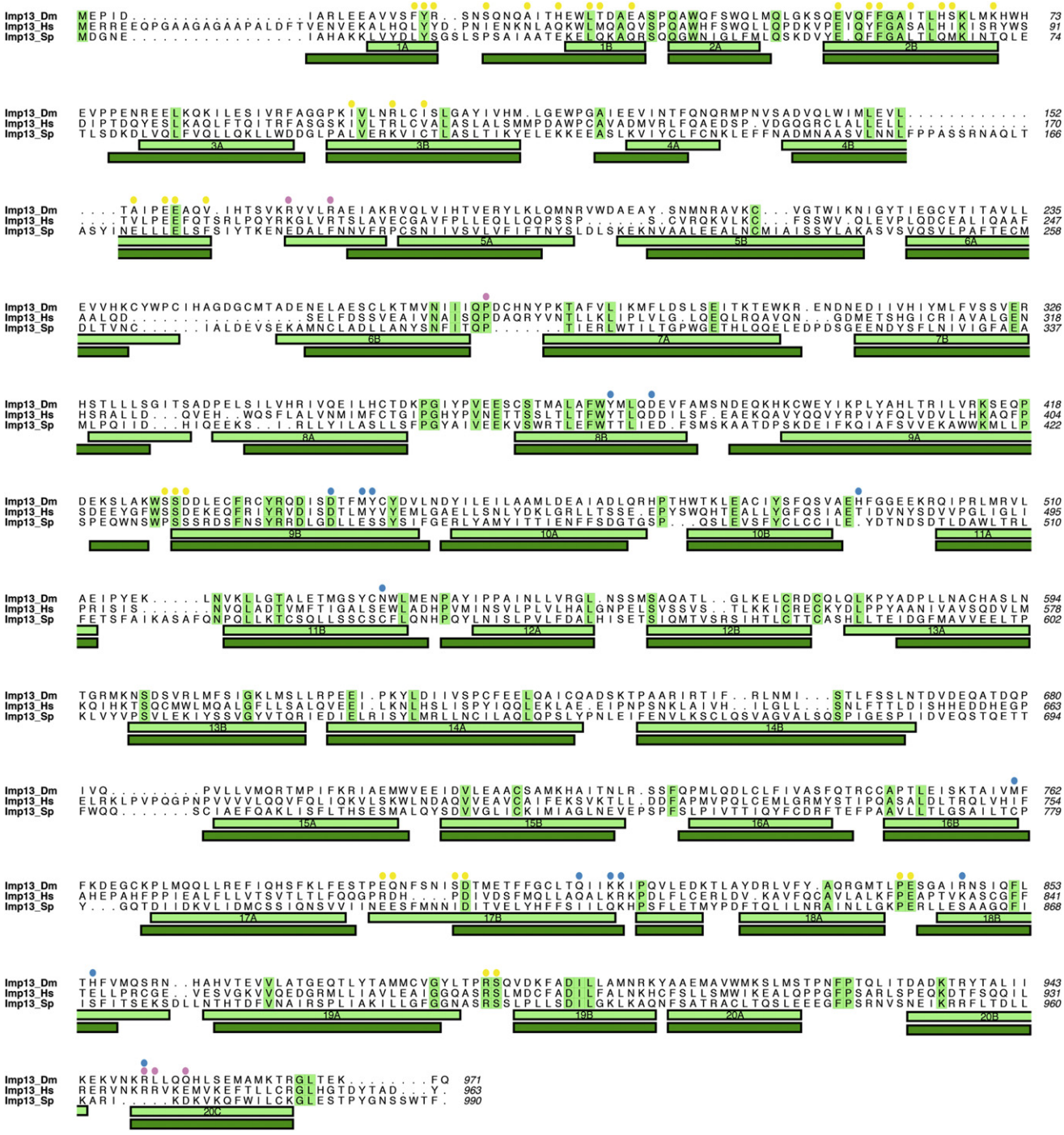

Figure 1. Structure-Based Sequence Alignment of Imp13

The alignment includes Imp13 orthologs from *D. melanogaster* (Dm), *H. sapiens* (Hs), and *S. pombe* (Sp). Highlighted in green are conserved residues. The secondary structure elements of Dm and Hs Imp13 are shown below the sequences as light and dark green rectangles, respectively. The A and B helices of the 20 HEAT repeats are labeled. Above the sequences, colored circles highlight the residues involved in the interaction with Mago (blue), Y14 (magenta), and Ran (yellow), as identified using the AquaProt server (Reichmann et al., 2007). See also Figure S1.

have similar secondary structure elements at similar positions in the sequence (Figure 1). Although the individual HEAT repeats of the two orthologs superpose with a root-mean-square deviation (rmsd) of 1.4 Å in their Cα atoms, the overall molecules superpose with a larger rmsd of 5.3 Å, reflecting the conformational differences in the two structures. The different conformations

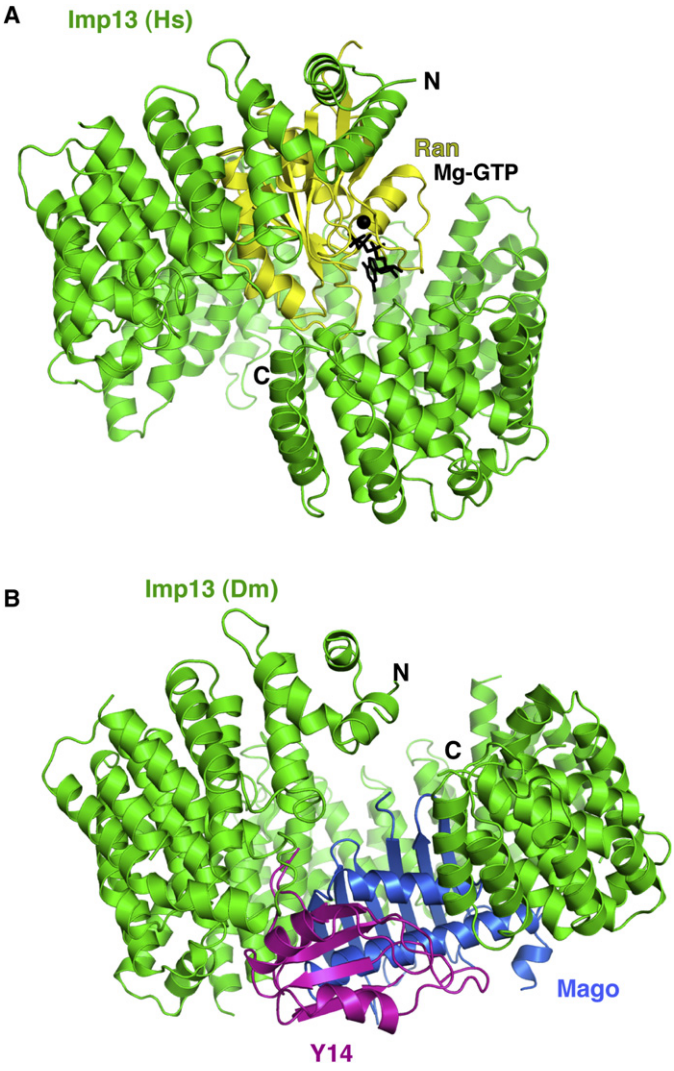

Figure 2. Structures of Imp13 Bound to the Cargo Mago-Y14 and to the Regulator Ran

(A) Structure of the Imp13-RanGTP complex. *H. sapiens* Imp13 is shown in green and Ran in yellow, with GTP and Mg^{2+} shown in ball-and-stick representation in black. The N terminus and C terminus of Imp13 are indicated. This and all other protein structure figures were generated using PyMOL (http://www.pymol.org). See also Figure S2.

(B) Structure of the Imp13-Mago-Y14 complex with *D. melanogaster* Imp13 in green, Mago in blue, and Y14 in magenta. The complex is shown in the same orientation as the RanGTP complex in (A), after optimal superposition of the karyopherin molecules.

result both from small cumulative shifts between individual HEAT repeats and from larger hinge movements.

Imp13 Binding to Mago-Y14: Snapshot of the Cytosolic Import Complex

In the complex with Imp13, Dm Mago-Y14 has a compact structure very similar to the previously reported structures of the Mago-Y14 heterodimer in isolation (rmsd of 0.98 Å over all Cα atoms) (Fribourg et al., 2003; Lau et al., 2003; Shi and Xu, 2003). Briefly, Mago is made up of a flat six-stranded antiparallel β sheet packed on one side by two long α helices (Figure 4). Y14 consists of a C-terminal region containing the fold of a canonical RRM (RNA-recognition motif) domain between residues 64 and 152, with a twisted antiparallel β sheet and two helices packing against one surface. The opposite surface of the Y14 β sheet (that is typically used by RRM domains to bind nucleic acids) interacts instead with the α helices of Mago.

In the complex with Imp13, there is no interpretable electron density for the N-terminal region of Y14. In the structure of full-length Dm Mago-Y14, the N-terminal region of Y14 was ordered between residues 10 and 39, with an α helix (residues 17–29) reaching over the β sheet surface of Mago diametrically opposite the RRM-binding surface (Fribourg et al., 2003). This conformation is not compatible with the Imp13-bound structure, as the N-terminal region of Y14 between residues 10 and 20 would clash with the B helix of HEAT 9 (Figure S4A). Thus, in the complex with Imp13, the N-terminal region of Y14 is displaced into a conformation that, from the features of the electron density, is likely to be flexible and to extend into the solvent. Consistent with this observation, in vitro pull-down experiments with recombinant proteins show that the N-terminal region of Y14 is not required for Imp13 binding (Figure S4B).

Mago fits into the arch of Imp13 formed between HEATs 8 and 20, with direct interactions at several positions (Figure 4). HEATs 8 and 9 contact one edge of the Mago β sheet (Figure 4A), at the site where the N terminus of Y14 was bound in the structure of Mago-Y14 in isolation (Fribourg et al., 2003). In particular, Asp443 of *D. melanogaster* Imp13 ($Asp443_{Dmi}$) approaches the side chain of Mago Arg34 ($Arg34_{M}$), while $Tyr447_{Dmi}$ and $Tyr378_{Dmi}$ contact the main chain. HEAT 15 contacts the Mago β sheet at the opposite side of the molecule, at $Leu76_{M}$, while HEATs 17 and 18 contact the nearby termini of the Mago α helices. In particular, $Lys815_{Dmi}$ and the adjacent $Lys814_{Dmi}$ point toward $Glu73_{M}$ and $Asp116_{M}$ (Figure 4B). Finally, HEAT 20 wraps up toward the side of the Mago α helices (Figure 4C). Here, the guanidinium groups of $Arg63_{M}$ and $Arg950_{Dmi}$ pack against each other. $Arg950_{Dmi}$ is in the very C-terminal helix of Imp13 and is also contacted at its main chain by Y14 Glu82 ($Glu82_{Y}$) and $Gln142_{Y}$.

Y14 is surrounded by the C-terminal HEATs 19 and 20 on one side and by HEATs 4–7 on the other. In particular, $Ile220_{Dmi}$ and $Pro275_{Dmi}$ at HEATs 5 and 6 are in van der Waals contacts with the side chains of $Leu128_{Y}$, $His124_{Y}$, and $Trp73_{Y}$, while $Glu132_{Y}$ approaches $Lys167_{Imp}$. Imp13 thus tightly and entirely encircles the Mago-Y14 heterodimer with many conserved interactions, explaining why purified Imp13 and Mago-Y14 can interact even across species (Figure S4B). Consistent with the structural analysis, mutation of $Lys815_{Dmi}$ and the adjacent $Lys814_{Dmi}$ (Figure 4B) to glutamate (thus reversing the charge) or mutation of $Tyr447_{Dmi}$ to arginine (Figure 4A) severely reduced the binding to Mago-Y14 in pull-down assays (Figure 4D, lanes 4 and 7, respectively).

Table 1. Crystallographic Statistics

Data collection			
Data set	Imp13-RanSeMet SAD	Imp13-Mago-Y14 native	Imp13-Mago-Y14 SeMet SAD
Beamline	SLS PX1	SLS PX2	SLS PX2
Space group	$P3_121$	$P1$	$P1$
Unit cell (Å)	a = b = 99.93, c = 276.52, $\alpha = \beta = 90°$, $\gamma = 120°$	a = 82.57, b = 100.79, c = 93.92, $\alpha = 89.83°$, $\beta = 110.18°$, $\gamma = 90.63°$	a = 83.28, b = 101.92,c = 94.25, $\alpha = 90.03°$, $\beta = 110.67°$, $\gamma = 89.92°$
Wavelength (Å)	0.978	0.978	0.979
Resolution range (Å)[a]	50–2.8 (3.0–2.8)	71–3.35 (3.53–3.35)	50–3.7 (3.9–3.7)
Unique reflections	76,082	39,374	29,677
Multiplicity	8.1	2.0	5.9
Completeness (%)[a]	100.0 (100.0)	96.3 (96.1)	97.1 (96.7)
Anomalous completeness (%)[a]	-	-	96.6 (96.1)
$I/\sigma(I)$[a]	15.3 (3.3)	5.7 (1.5)	9.2 (3.1)
R_{sym}(%)[a]	10.0 (66.9)	9.8 (56.0)	15.0 (55.9)
Phasing			
R_{cullis}(%)[a]	-	-	-
Phasing power	-	-	-
Refinement			
Resolution range (Å)[a]	50–2.80	50–3.35	-
R_{free} (%)[a]	26.8	28.9	-
R_{work} (%)[a]	23.6	26.7	-
Rmsd bond (Å)	0.008	0.006	-
Rmsd angle (°)	1.37	1.25	-
B factor protein ($Å^2$)	69.9	97.3	-
B factor ligands ($Å^2$)	-	-	-
Ramachandran values			
Most favored (%)	92.6	90.5	-
Additionally allowed (%)	7.4	9.5	-
Generously allowed (%)	0	0	-
Disallowed (%)	0	0	-

[a] Values in parentheses correspond to the highest-resolution shell.

Imp13 Binding to Ran: Snapshot of the Nuclear State

RanGTP has a compact core domain with a Ras-like fold that has been extensively described with previous crystal structures (Chook and Blobel, 1999; Vetter et al., 1999). The core domain features two regions that interact with the bound GTP, the switch I region (residues Thr34–Val47, yeast numbering) and switch II region (residues Thr68–Tyr82), so called because they switch conformation when the nucleotide is hydrolyzed (Milburn et al., 1990). These regions interact with two distinct surfaces of Imp13. Switch I binds the C-terminal portion of Imp13 at HEAT motifs 16–19 (Figure 5A). The interaction occurs mainly via polar and electrostatic contacts, in particular between $Lys39_{Ran}$ and $Lys40_{Ran}$ approaching $Asp785_{Hsl}$ and $Asp788_{Hsl}$. Switch II contacts the N-terminal portion of Imp13 at HEAT 1–3, with hydrophobic contacts centered at $Leu77_{Ran}$ and electrostatic contacts between $Asp79_{Ran}$ and $Arg122_{Hsl}$ (Figure 5A). The helix adjacent to switch II in the core domain contacts HEATs 3 and 4, in particular with $Arg108_{Ran}$ and $Arg112_{Ran}$ approaching $Glu175_{Hsl}$ and $Glu176_{Hsl}$. RanGTP also establishes a third interaction with the central portion of Imp13 at HEATs 8 and 9, with $Arg168_{Ran}$ and $Lys169_{Ran}$ approaching $Asp415_{Hsl}$ and $Glu416_{Hsl}$ on helix 9B (Figure 5B).

The mode of Ran binding to the N-terminal region of Imp13 is largely similar to that observed with other members of the karyopherin family, which indeed share the highest degree of conservation in the N-terminal half of the molecule (Görlich et al., 1997). The interaction in the middle region of Imp13 centered at HEAT 9 is also found in most other karyopherins, although the details differ. In importin β and transportin, this contact is mediated by a conserved acidic loop within HEAT 8 (Chook and Blobel, 1999; Lee et al., 2005). Imp13 has no such loop, but the negatively charged residues in the B helix of HEAT 9 reside in a similar structural position and serve a similar purpose. Imp13 is, in this sense, more similar to the exportins Crm1 and Cse1 (Dong et al., 2009; Matsuura and Stewart, 2004; Monecke et al., 2009). Finally, the interaction of RanGTP with the C-terminal HEATs diverges among the karyopherins studied to date. While Ran docks at HEAT 16–19 in the case of Imp13 and Crm1, it binds to HEAT 14 and 15 in the case of importin β and Cse1. These differences are reflected in the overall superhelical conformation of the karyopherins, with Imp13

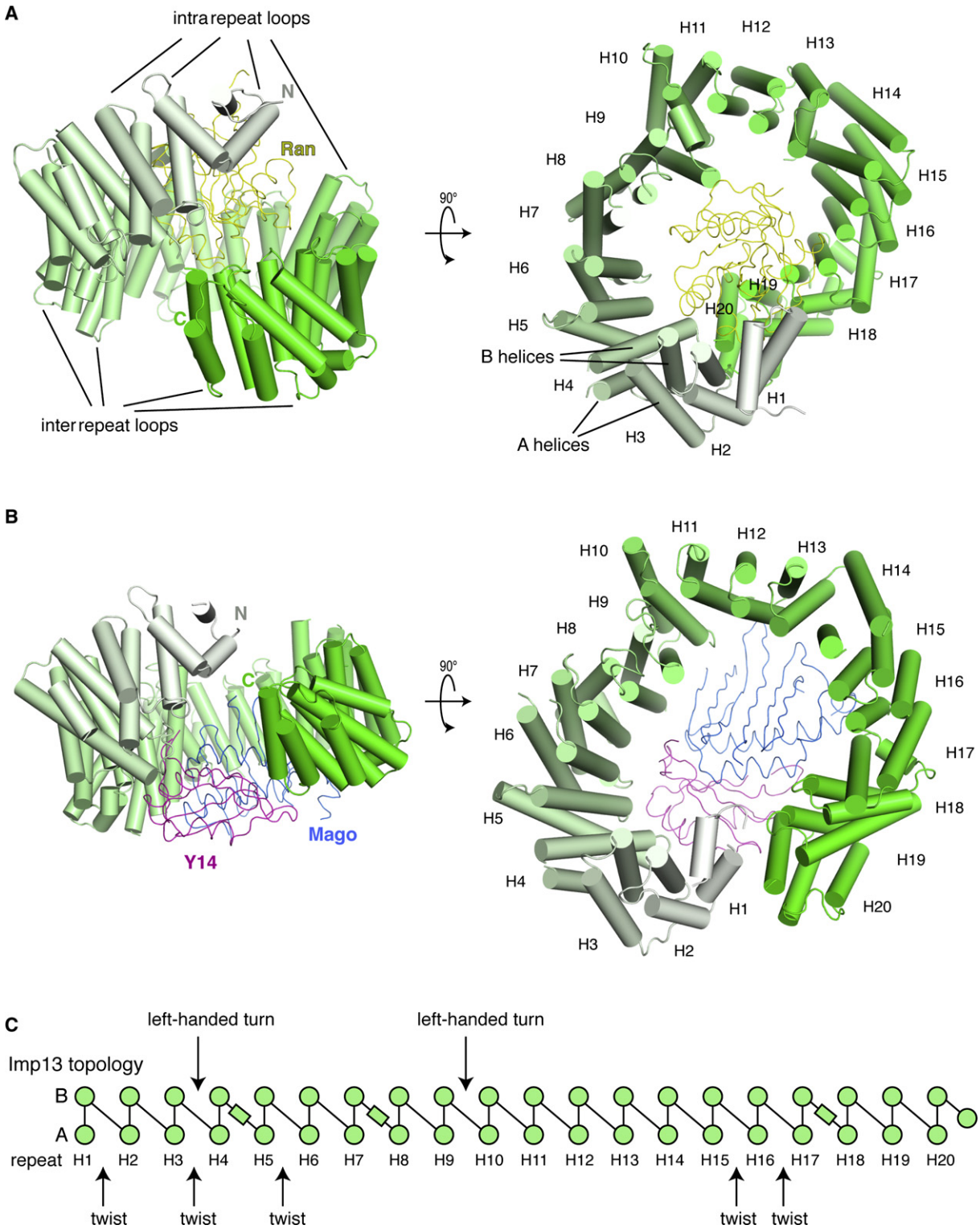

Figure 3. Conformational Variability of Imp13

(A) The Imp13-RanGTP complex is viewed in two orientations related by a 90° rotation around a horizontal axis, with the α helices of the Imp13 HEAT repeats shown as cylinders and colored with a gradient from gray (N terminus) to green (C terminus). The orientation in the left panel is the same as in Figure 2A. The HEAT repeats, as well as two of the A and B helices, are labeled on the right panel. Some of the intra- and interrepeat loops are indicated on the left panel. Ran is visible in a ribbon representation in yellow. See also Figure S3.

and Crm1 curling up in a more closed conformation than importin β and Cse1. Along the same lines, transportin makes only limited contacts with Ran at HEAT 14 and 15, and the superhelix is the most extended in comparison to the other karyopherin-β structures (Chook and Blobel, 1999) (Figure S3).

Mechanisms of Ran Dissociation and Cargo Release from Imp13

The RanGTP-bound state of Imp13 changes when the complex reaches the cytosol: as GTP is hydrolyzed to GDP, Ran dissociates from Imp13. Superposition of the RanGDP structure to the Imp13-RanGTP complex shows that the conformation of switch I and of the C-terminal tail of Ran (known as switch III) has the greatest impact on Imp13 binding. In the GDP-bound conformation, the contact between HEATs 17 and 18 to the switch I region would be lost, and this switch region would assume a conformation that would clash with HEAT 1 of Imp13 (Figure S5A). In addition, the C-terminal tail of Ran (which is known to be unstructured in the GTP-bound form and which was removed from the construct that crystallized) would assume a stable helical conformation on the surface of the Ran core domain that would clash with HEAT 9. Thus, the collapse of the Ran-bound Imp13 complex upon hydrolysis to RanGDP relies on a similar molecular mechanism observed in other karyopherins (Chook and Blobel, 1999; Cook et al., 2009; Lee et al., 2005; Monecke et al., 2009; Vetter et al., 1999).

Conversely, the cargo-bound state of Imp13 changes when the complex reaches the nucleus: upon RanGTP binding to Imp13, Mago-Y14 is dissociated. In the two importins studied to date, importin β and transportin, cargo release relies on their characteristic acidic loop at HEAT 8 (Cingolani et al., 1999; Lee et al., 2006). However, as described above, Imp13 lacks this structural feature, and therefore cargo release is likely to be mediated by a different molecular mechanism. Comparison of the structures of Imp13 bound to RanGTP and bound to Mago-Y14 shows that the GTPase and the cargo interact with different surface residues of the karyopherins and therefore do not compete for the same binding sites. The reverse-charge double mutation of $Lys814_{Dmi}$ and $Lys815_{Dmi}$, for example, impairs Mago-Y14 binding (Figure 4D, lane 4) but does not abolish Ran binding (Figure S5B). When the two structures are superposed, RanGTP and Mago-Y14 assume an almost side-by-side position when bound to Imp13, but concomitant binding would not be possible, as they would be too close: the loops on one side of the Mago β sheet would clash against the loops of the Ran β sheet (Figure 6A). As expected, increasing amounts of RanGTP progressively decrease the amount of Mago-Y14 binding to GST-Imp13 in pull-down experiments (Figure S5C).

Mutually Exclusive Binding of Mago-Y14 to Either Imp13 or PYM

Mago-Y14 is a nuclear protein at steady state, but shuttles to the cytoplasm as part of the mRNA-associated EJC (Le Hir et al., 2001). It has recently been reported, using in vitro splicing reactions and immunoprecipitations, that the protein PYM is involved in EJC dissociation (Gehring et al., 2009b), consistent with previous reports suggesting that PYM binding to Mago-Y14 would not be compatible in the context of the EJC (Bono et al., 2006). The N-terminal domain of PYM binds Mago-Y14 at a composite surface formed by a loop of the Y14 RRM (known as the β2-β3 loop) and by the α helices of Mago (Bono et al., 2004). In particular, PYM docks with electrostatic interactions at the negatively charged surface of the Mago α helices centered at $Glu73_M$. This surface is also used to bind Imp13. Superposition of the structures of Mago-Y14 bound to Imp13 and to PYM shows that Arg18 and Arg24 of PYM occupy a similar position in space as Lys815 and Lys814 of Imp13 (Figure 6B). Thus, the two interactions are mutually exclusive, as the β hairpin of PYM (residues 15–24) would clash with HEAT 16, 17, and 18 of Imp13. This prediction from the structure can be recapitulated biochemically. A reverse-charged mutation of Mago Glu73 to arginine impairs the interaction either with Imp13 or PYM (Figure 6C). Moreover, increasing amounts of Imp13 progressively reduce the amounts of PYM binding to GST-Mago-Y14 in competition experiments (Figure 6D).

Conclusions

A challenge in understanding how mRNPs function at the molecular level is to decipher how and when the composition of the protein components changes during their complex life cycle. mRNP dynamics are the result of different cellular machineries, which act with a precise sequence of events that depend on concomitant or incompatible interactions. Mago and Y14 participate in a complex set of sequential binding events: they assemble into the EJC to associate with mRNPs in the nucleus, bind to PYM during or after EJC dissociation in the cytoplasm, bind to Imp13 to return back to the nucleus, and are dissociated from it by RanGTP (Figure S6). Previous work had elucidated the first steps of the Mago-Y14 pathway at the atomic level, revealing the intricate network of interactions that form the RNA-bound EJC and its mutually exclusive interactions with PYM (Andersen et al., 2006; Bono et al., 2004, 2006). We now report the mechanisms of the nuclear import step of the cycle. Mago-Y14 is recognized by the karyopherin Imp13 via specific and evolutionarily conserved contacts. The transport factor forms a ring around the Mago-Y14 cargo, binding at a surface that is also used for PYM recognition. Concomitant binding of PYM is thus sterically incompatible, explaining how this Mago-Y14-binding partner is excluded from the nuclear import step. Similarly, Mago-Y14 is sterically inaccessible to Imp13 when in the EJC.

Binding of RanGTP in the nucleus successively displaces Mago-Y14 from the transport factor. The sites at which RanGTP binds on the karyopherin are mostly accessible in the Imp13-Mago-Y14 complex, providing a rationale for how the GTPase would be able to approach and dock to the transport factor as

(B) The Imp13-Mago-Y14 complex is shown with similar views and representations as the RanGTP complex in (A). Mago and Y14 are visible in a ribbon representation in blue and magenta.
(C) Schematic of the Dm Imp13 secondary structure, with the A and B helices of each HEAT repeat indicated. Two left-handed turns are indicated, as are disruptions between subsequent HEAT repeats that differ between the two structures (twists).

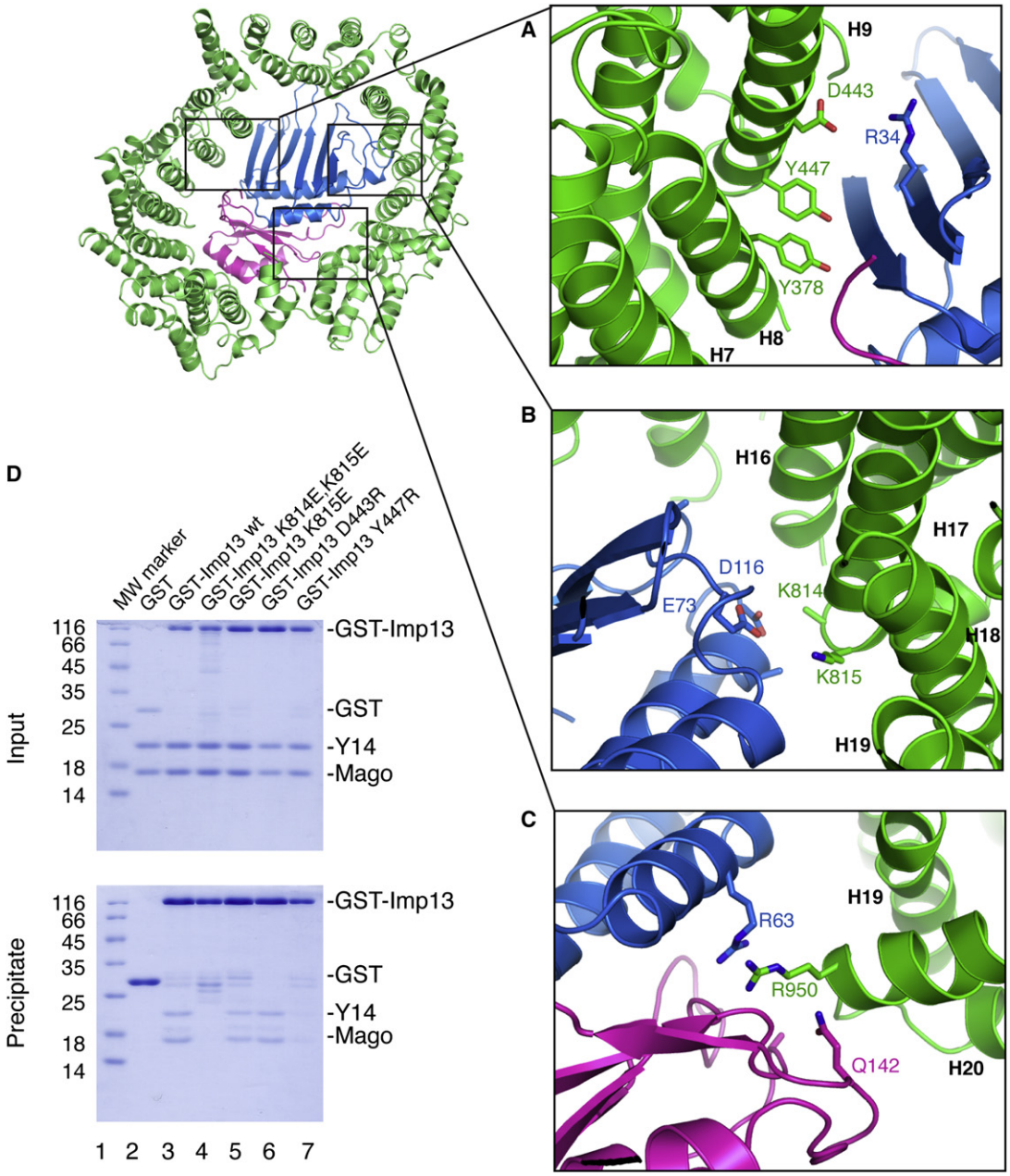

Figure 4. Conserved Interactions between Imp13 and Mago-Y14

(A–C) Close-up views of the interactions between Imp13 and Mago-Y14. The molecules are in a similar orientation as in Figure 3B, right panel. The views show the interaction between HEATs 8 and 9 of Imp13 and the Mago β sheet (A), between HEATs 17 and 18 of Imp13 and the Mago loops (B), and between HEAT 20 and the interface of the Mago-Y14 heterodimer (C). Residues of Imp13 are labeled in green, of Mago in blue, and of Y14 in magenta, and HEAT repeats are in black (bold). See also Figure S4.

(D) Protein coprecipitations by GST pull-down assays. GST-tagged *Drosophila* Imp13 wild-type or mutants were incubated with full-length Mago-Y14 in a buffer containing 50 mM NaCl. One-sixth of the sample was kept as input control (upper panel), and the rest was coprecipitated with glutathione-Sepharose beads (lower panel). Both input and pull-down samples were analyzed on Coomassie-stained 15% SDS-PAGE. Lane 1 shows binding to GST as control. The far left lane was loaded with a molecular weight marker.

it enters the nucleus in a complex. When fully bound, RanGTP binding would sterically push Mago-Y14 out of the complex: although the binding sites for cargo and Ran are positioned roughly side-by-side on the karyopherin, the molecules would come into too close a contact with each other for their binding to be simultaneous. In this scenario, it is possible to envisage how this unusual karyopherin might be able to mediate bidirectional transport, rather than being a canonical unidirectional

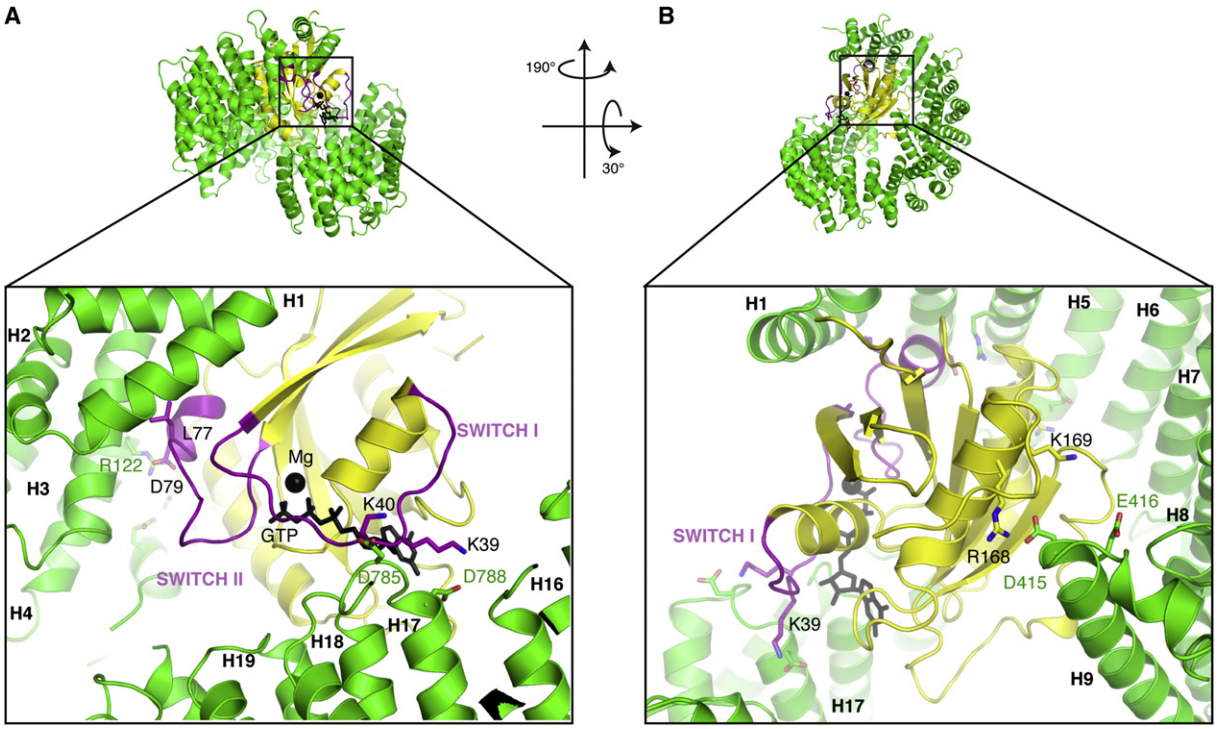

Figure 5. Conserved Interactions between Imp13 and Ran

(A) Close-up view of the interaction between the switch I region of Ran and HEATs 17 and 18 and between the switch II region of Ran and HEATs 3 and 4. The molecule is shown in the same orientation as in Figure 3A, left panel. Ran is in yellow, the switch regions in violet, and GTP and Mg in black. Residues of Imp13 are labeled in green, residues of Ran in black, and HEAT repeats are in black (bold). See also Figure S5.

(B) Close-up view of the interaction between Ran and HEATs 8 and 9 of Imp13. The molecule is shown in the same orientation as in Figure 3A, right panel.

import or export factor. An export cargo might also bind to Imp13 with a side-by-side configuration relative to Ran but occupy less space than Mago-Y14, so as not to clash with RanGTP and to require the proximity with RanGTP for increasing its binding affinity. In this situation, Imp13 would be able to mediate either the cooperative or antagonistic binding of Ran with the cargo depending on its specific structural features. This would in turn define whether a cargo is destined for import or export.

EXPERIMENTAL PROCEDURES

Protein Expression and Purification

D. melanogaster Mago and Y14 were coexpressed in *E. coli* and purified essentially as previously described (Fribourg et al., 2003). Dm *Imp13* was cloned from a full-length commercial (Drosophila Genomics Resource Center) clone and the Hs *Imp13* clone was a kind gift from Dirk Görlich (MPI; Goettingen, Germany). Dm and Hs Imp13 were expressed as N-terminal GST fusion proteins in *E. coli* BL21-GOLD pLysS cells (Stratagene; Amsterdam Zudoost, Holland) with an overnight induction at 18°C. They were affinity-purified on glutathione-Sepharose beads (GE Healthcare; Freiburg, Germany) in buffer A (20 mM Tris [pH 7.5], 100 mM NaCl, 1 mM dithiothreitol [DTT]). Binding to the resin was performed in batch, and the tag was removed by addition of Tobacco Etch Virus (TEV) protease. The cleaved proteins were further purified by anion-exchange chromatography using a HiQ column (Bio-Rad; Munich, Germany) in buffer A and eluted with a gradient of 100–750 mM NaCl. The Dm Imp13-Mago-Y14 complex was formed by adding a 1.5-fold excess of pure Mago-Y14 heterodimer to Imp13 and incubating for 2 hr at 4°C prior to loading the complex onto a Superdex 200 gel filtration column (GE Healthcare). Attempts to measure the affinity of the interaction between GST-Imp13 and Mago-Y14 either by surface plasmon resonance (SPR) or by isothermal titration calorimetry (ITC) failed, mainly because a significant percentage of Imp13 aggregates over time (as detected in static light scattering [SLS] measurements) (data not shown).

A construct of yeast RanQ71L encompassing residues 8–179 was expressed as an N-terminal His-tagged protein in *E. coli* BL21-GOLD pLysS cells with an overnight induction at 18°C. His-tagged Ran was purified by Ni^{2+}-NTA chromatography with buffer B (20 mM Tris [pH 7.5], 4 mM $MgCl_2$, 10% glycerol, and 0.5 mM DTT) supplemented with 500 mM NaCl and 5 mM imidazole. After elution (buffer B with 500 mM NaCl, 500 mM imidazole, and 1 mM β-mercaptoethanol), the protein was dialyzed in the presence of TEV protease (buffer B with 250 mM NaCl and with 1 mg TEV per 50 mg Ran). It was then loaded on a Co^{2+}-Talon (Clontech; Saint-Germain-en-Laye, France) column and collected in the flowthrough. To ensure the formation of a homogeneous nucleotide-bound state of Ran, the pure protein was incubated with 7 mM EDTA, dialyzed in buffer B supplemented with 50 mM NaCl, and then incubated with a 5-fold molar excess of GTP and 10 mM $MgCl_2$ at room temperature for 30 min. As a final purification step, RanGTP was purified by cation-exchange chromatography (ResourceS, GE Healthcare) in buffer B and eluted with a 1 M NaCl gradient. The Imp13-Ran complex was formed by adding a 1.5-fold molar excess of Ran to Imp13 for 2 hr at 4°C. The 1:1 complex was then purified on a Superdex 200 size-exclusion column.

For phasing, Hs and Dm Imp13 proteins labeled with SeMet were used to form the corresponding complexes with either unlabeled RanGTP or unlabelled Mago-Y14. The SeMet-labeled Imp13 proteins were expressed in BL21-GOLD pLysS cells grown in M9 minimal media and starved before addition of SeMet (Van Duyne et al., 1993). They were purified with the same protocol used for the unmodified proteins.

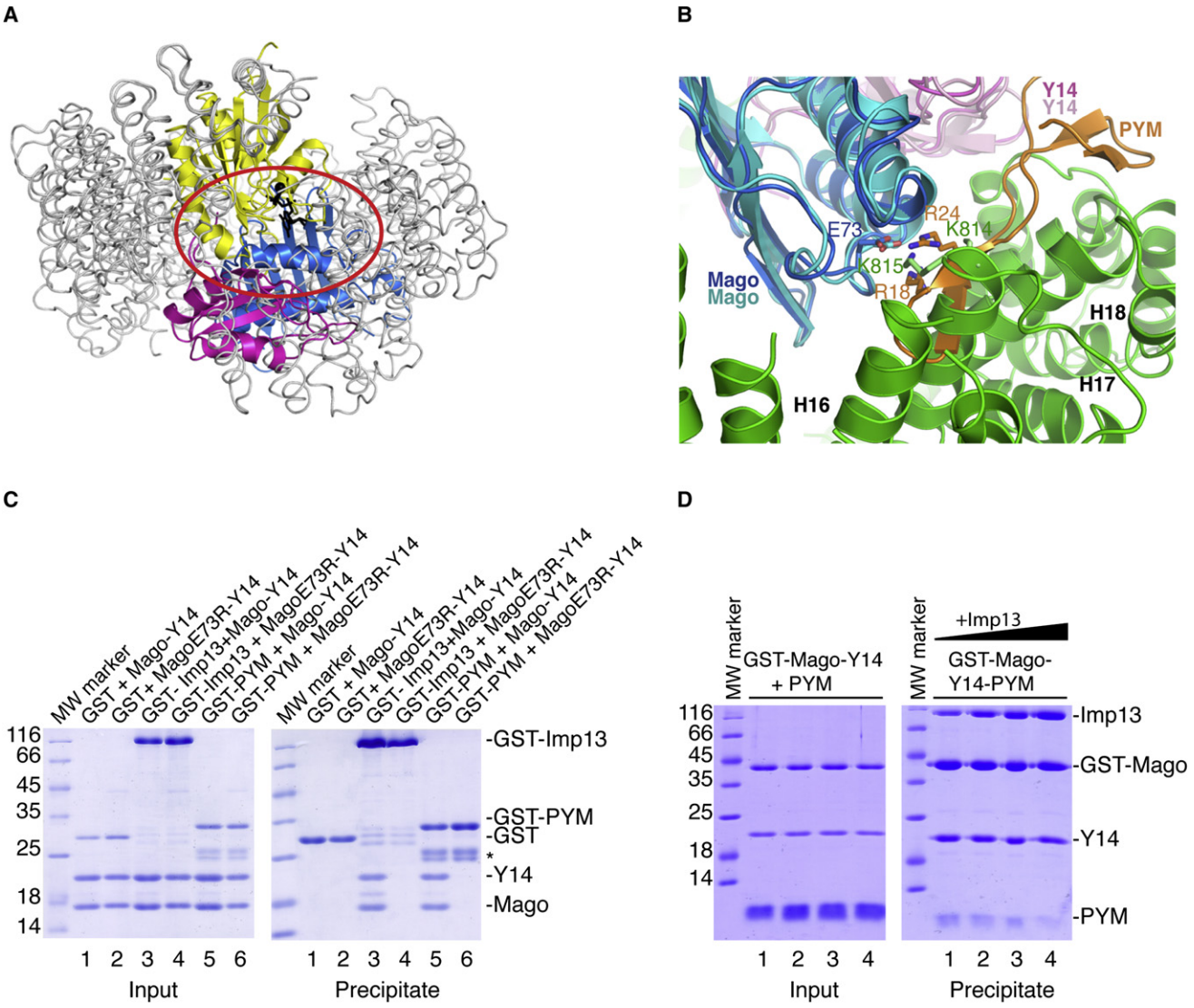

Figure 6. Mutually Exclusive Interactions on Imp13 and Mago-Y14

(A) Superposition of the structures of Imp13-Mago-Y14 and Imp13-RanGTP. The molecules are viewed in the same orientation as in Figure 2, with Imp13 shown in a ribbon representation in gray. Although Mago-Y14 and RanGTP bind to a large extent to different regions of Imp13, their concomitant binding would result in steric clashes (region highlighted with a red circle). See also Figure S6.

(B) Superposition of the structures of Imp13-Mago-Y14 and Mago-Y14-PYM. Imp13 (green) and PYM (orange) interact with the same region of Mago (blue) centered at Glu73. HEAT repeats are labeled in black (bold).

(C) Protein coprecipitations by GST pull-down assays. *Drosophila* GST-tagged Imp13 or GST-tagged PYM were incubated with full-length Mago-Y14, either wild-type or containing the Mago E73R mutation. The pull-downs were carried out with a similar protocol described in Figure 4D. The input and precipitated samples are shown in the left and right panels. The leftmost lanes were loaded with a molecular weight marker. Bands marked with an asterisk are degradation impurities of GST-PYM.

(D) Competition experiments showing the effect of Imp13 on the PYM-binding properties of Mago-Y14. GST-Mago-Y14 was incubated on beads with an excess of PYM (input, left panel). After washing, increasing amounts of Imp13 (from 2.3 μg in lane 1 to 13.8 μg in lane 4) were added in the pull-down. The competition experiments are representative of five repetitions, all showing that the amount of Imp13 precipitated is progressively increased while the amount of PYM is progressively decreased.

Crystallization, Data Collection, and Structure Determination

Crystallization experiments were carried out using the vapor diffusion method. The best crystals of the Imp13-RanGTP complex were obtained at 18°C using a reservoir solution containing 100 mM Bis-Tris (pH 6.0), 23% (w/v) PEG 3350, and 100 mM Na-thiocyanate. For data collection, the crystals were flash-cooled in liquid nitrogen after addition of 20% glycerol as cryoprotectant to the reservoir solution. The crystals diffracted to 2.8 Å resolution at the PXII beamline of the Swiss Light Source (Villigen, Switzerland). They belong to space group $P3_121$ with cell dimensions $a = b = 99.93$ Å, $c = 276.52$ Å and contain one molecule in the ASU. Diffraction data were processed with the program XDS (Kabsch, 1993). The structure was solved by SeMet SAD phasing. SHELX (Schneider and Sheldrick, 2002) was used to obtain 23 selenium sites and initial phases. Model building was carried out with Coot (Emsley and Cowtan, 2004) and alternating cycles of refinement with CNS (Brünger et al., 1998).

Initial crystals of the Imp13-Mago-Y14 complex were obtained using 100 mM MES (pH 6.5) and 26% (v/v) PEG 300 as reservoir solution and were optimized with the addition of 6% trimethylamine N-oxide dihydrate and by microseeding. The crystals were flash-cooled in liquid nitrogen after adding 40% (v/v) PEG 400. Diffraction data to 3.35 Å resolution were collected at the SLS synchrotron and were processed with the program XDS (Kabsch, 1993). The crystals belong to space group *P*1 with cell dimensions a = 82.6 Å, b = 100.8 Å, c = 93.9 Å and α = 89.8°, β = 110.2°, γ = 90.6°. The ASU of the crystals contains two independent copies of the Imp13-Mago-Y14 complex related by a noncrystallographic two-fold axis. The structure was solved with the program Phaser (McCoy et al., 2007) using a combination of molecular replacement and single-wavelength anomalous dispersion (SAD) data on a crystal grown using SeMet-substituted Imp13. Phased molecular replacement in Phaser using the structure of *Drosophila* Mago-Y14 as search model (PDB code 1HL6) allowed the location of 41 of the expected 86 selenium sites and gave initial phases. The electron density was improved with DM (CCP4, 1994), model building was performed with the program O (Jones and Kjeldgaard, 1997), and refinement with CNS (Brünger et al., 1998).

In Vitro Binding Assays

In the pull-down assays in Figures 4D and 6C, GST-tagged recombinant Imp13 or PYM proteins and purified binding partners (2 μg of each) were mixed in binding buffer (20 mM HEPES [pH 7.5], 50 mM NaCl, 1 mM DTT, 10% glycerol, 0.1% [v/v] Nonidet P40) to a final volume of 60 μl and incubated for 1 hr at 4°C. Complexes were immobilized on 15 μl glutathione agarose beads (GE Healthcare) and incubated for 1 hr at 4°C. The resin was washed three times with 500 μl binding buffer and eluted with 20 mM reduced glutathione in elution buffer (30 mM Tris-HCl [pH 8.8], 150 mM NaCl, 1 mM DTT, 14% glycerol, 0.1% [v/v] Nonidet P40). Eluates were dried down, mixed with SDS loading buffer, boiled, and loaded on 15% SDS-PAGE with a protein molecular mass marker. Proteins were visualized by Coomassie staining. In the competition experiment in Figure 6D, 4 μg GST-Mago-Y14 and PYM was incubated on beads and washed, and increasing amounts of Imp13 were added (2.3 μg, 4.6 μg, 9.2 μg, and 13.8 μg from lanes 1 to 4).

ACCESSION NUMBERS

The coordinates and structure factors have been deposited in the Macromolecular Structure Database of the European Bioinformatic Institute (EBI) with ID code 2x19 (Imp13-RanGTP complex) and 2x1g (Imp13-Mago-Y14 complex).

SUPPLEMENTAL INFORMATION

Supplemental Information includes six figures and can be found with this article online at doi:10.1016/j.molcel.2010.01.007.

ACKNOWLEDGMENTS

We would like to thank Petra Birle and Tatjana Krywcun for mutagenesis and Jerome Basquin, Karina Valer Saldana, and Sabine Pleyer at the MPI-Martinsried crystallization facility. We also thank Dirk Görlich for the Hs Imp13 clone, the staff of the PX beamlines at the Swiss Light Source (Villigen, Switzerland) for assistance during data collection, and Randy Read for suggestions with Phaser. We thank members of the lab, Esben Lorentzen and Elisa Izaurralde, for suggestions and critical reading of the manuscript. This study was supported by the Max Planck Gesellschaft, the EU grant 3D Repertoire (contract number LSHG-CT-2005-51202), the Sonderforschungsbereich SFB646, and the Gottfried Wilhelm Leibniz Program of the Deutsche Forschungsgemeinschaft (DFG).

Received: October 6, 2009
Revised: December 2, 2009
Accepted: January 6, 2010
Published: January 28, 2010

REFERENCES

Andersen, C.B., Ballut, L., Johansen, J.S., Chamieh, H., Nielsen, K.H., Oliveira, C.L., Pedersen, J.S., Séraphin, B., Le Hir, H., and Andersen, G.R. (2006). Structure of the exon junction core complex with a trapped DEAD-box ATPase bound to RNA. Science *313*, 1968–1972.

Ballut, L., Marchadier, B., Baguet, A., Tomasetto, C., Séraphin, B., and Le Hir, H. (2005). The exon junction core complex is locked onto RNA by inhibition of eIF4AIII ATPase activity. Nat. Struct. Mol. Biol. *12*, 861–869.

Bischoff, F.R., Klebe, C., Kretschmer, J., Wittinghofer, A., and Ponstingl, H. (1994). RanGAP1 induces GTPase activity of nuclear Ras-related Ran. Proc. Natl. Acad. Sci. USA *91*, 2587–2591.

Bono, F., Ebert, J., Unterholzner, L., Güttler, T., Izaurralde, E., and Conti, E. (2004). Molecular insights into the interaction of PYM with the Mago-Y14 core of the exon junction complex. EMBO Rep. *5*, 304–310.

Bono, F., Ebert, J., Lorentzen, E., and Conti, E. (2006). The crystal structure of the exon junction complex reveals how it maintains a stable grip on mRNA. Cell *126*, 713–725.

Brünger, A.T., Adams, P.D., Clore, G.M., DeLano, W.L., Gros, P., Grosse-Kunstleve, R.W., Jiang, J.S., Kuszewski, J., Nilges, M., Pannu, N.S., et al. (1998). Crystallography & NMR system: A new software suite for macromolecular structure determination. Acta Crystallogr. D Biol. Crystallogr. *54*, 905–921.

Chamieh, H., Ballut, L., Bonneau, F., and Le Hir, H. (2008). NMD factors UPF2 and UPF3 bridge UPF1 to the exon junction complex and stimulate its RNA helicase activity. Nat. Struct. Mol. Biol. *15*, 85–93.

Chook, Y.M., and Blobel, G. (1999). Structure of the nuclear transport complex karyopherin-beta2-Ran x GppNHp. Nature *399*, 230–237.

Cingolani, G., Petosa, C., Weis, K., and Müller, C.W. (1999). Structure of importin-beta bound to the IBB domain of importin-alpha. Nature *399*, 221–229.

CCP4 (Collaborative Computational Project, Number 4). (1994). The CCP4 suite: programs for protein crystallography. Acta Crystallogr. D Biol. Crystallogr. *50*, 760–763.

Cook, A., Fernandez, E., Lindner, D., Ebert, J., Schlenstedt, G., and Conti, E. (2005). The structure of the nuclear export receptor Cse1 in its cytosolic state reveals a closed conformation incompatible with cargo binding. Mol. Cell *18*, 355–367.

Cook, A., Bono, F., Jinek, M., and Conti, E. (2007). Structural biology of nucleocytoplasmic transport. Annu. Rev. Biochem. *76*, 647–671.

Cook, A.G., Fukuhara, N., Jinek, M., and Conti, E. (2009). Structures of the tRNA export factor in the nuclear and cytosolic states. Nature *461*, 60–65.

Diem, M.D., Chan, C.C., Younis, I., and Dreyfuss, G. (2007). PYM binds the cytoplasmic exon-junction complex and ribosomes to enhance translation of spliced mRNAs. Nat. Struct. Mol. Biol. *14*, 1173–1179.

Dong, X., Biswas, A., Süel, K.E., Jackson, L.K., Martinez, R., Gu, H., and Chook, Y.M. (2009). Structural basis for leucine-rich nuclear export signal recognition by CRM1. Nature *458*, 1136–1141.

Emsley, P., and Cowtan, K. (2004). Coot: model-building tools for molecular graphics. Acta Crystallogr. D Biol. Crystallogr. *60*, 2126–2132.

Forler, D., Köcher, T., Rode, M., Gentzel, M., Izaurralde, E., and Wilm, M. (2003). An efficient protein complex purification method for functional proteomics in higher eukaryotes. Nat. Biotechnol. *21*, 89–92.

Fribourg, S., Gatfield, D., Izaurralde, E., and Conti, E. (2003). A novel mode of RBD-protein recognition in the Y14-Mago complex. Nat. Struct. Biol. *10*, 433–439.

Gehring, N.H., Lamprinaki, S., Hentze, M.W., and Kulozik, A.E. (2009a). The hierarchy of exon-junction complex assembly by the spliceosome explains key features of mammalian nonsense-mediated mRNA decay. PLoS Biol. *7*, e1000120.

Gehring, N.H., Lamprinaki, S., Kulozik, A.E., and Hentze, M.W. (2009b). Disassembly of exon junction complexes by PYM. Cell *137*, 536–548.

Giagtzoglou, N., Lin, Y.Q., Haueter, C., and Bellen, H.J. (2009). Importin 13 regulates neurotransmitter release at the Drosophila neuromuscular junction. J. Neurosci. *29*, 5628–5639.

Giorgi, C., and Moore, M.J. (2007). The nuclear nurture and cytoplasmic nature of localized mRNPs. Semin. Cell Dev. Biol. *18*, 186–193.

Görlich, D., and Kutay, U. (1999). Transport between the cell nucleus and the cytoplasm. Annu. Rev. Cell Dev. Biol. *15*, 607–660.

Görlich, D., Dabrowski, M., Bischoff, F.R., Kutay, U., Bork, P., Hartmann, E., Prehn, S., and Izaurralde, E. (1997). A novel class of RanGTP binding proteins. J. Cell Biol. *138*, 65–80.

Herold, N., Will, C.L., Wolf, E., Kastner, B., Urlaub, H., and Lührmann, R. (2009). Conservation of the protein composition and electron microscopy structure of Drosophila melanogaster and human spliceosomal complexes. Mol. Cell. Biol. *29*, 281–301.

Jones, T.A., and Kjeldgaard, M. (1997). Electron-density map interpretation. Methods Enzymol. *277*, 173–208.

Kabsch, W. (1993). Automatic processing of rotation diffraction data from crystals of initially unknown symmetry and cell constants. J. Appl. Cryst. *26*, 795–800.

Lau, C.K., Diem, M.D., Dreyfuss, G., and Van Duyne, G.D. (2003). Structure of the Y14-Magoh core of the exon junction complex. Curr. Biol. *13*, 933–941.

Le Hir, H., Izaurralde, E., Maquat, L.E., and Moore, M.J. (2000). The spliceosome deposits multiple proteins 20-24 nucleotides upstream of mRNA exon-exon junctions. EMBO J. *19*, 6860–6869.

Le Hir, H., Gatfield, D., Braun, I.C., Forler, D., and Izaurralde, E. (2001). The protein Mago provides a link between splicing and mRNA localization. EMBO Rep. *2*, 1119–1124.

Lee, S.J., Matsuura, Y., Liu, S.M., and Stewart, M. (2005). Structural basis for nuclear import complex dissociation by RanGTP. Nature *435*, 693–696.

Lee, B.J., Cansizoglu, A.E., Süel, K.E., Louis, T.H., Zhang, Z., and Chook, Y.M. (2006). Rules for nuclear localization sequence recognition by karyopherin beta 2. Cell *126*, 543–558.

Matsuura, Y., and Stewart, M. (2004). Structural basis for the assembly of a nuclear export complex. Nature *432*, 872–877.

McCoy, A.J., Grosse-Kunstleve, R.W., Adams, P.D., Winn, M.D., Storoni, L.C., and Read, R.J. (2007). Phaser crystallographic software. J. Appl. Cryst. *40*, 658–674.

Milburn, M.V., Tong, L., deVos, A.M., Brünger, A., Yamaizumi, Z., Nishimura, S., and Kim, S.H. (1990). Molecular switch for signal transduction: structural differences between active and inactive forms of protooncogenic ras proteins. Science *247*, 939–945.

Mingot, J.M., Kostka, S., Kraft, R., Hartmann, E., and Görlich, D. (2001). Importin 13: a novel mediator of nuclear import and export. EMBO J. *20*, 3685–3694.

Monecke, T., Güttler, T., Neumann, P., Dickmanns, A., Görlich, D., and Ficner, R. (2009). Crystal structure of the nuclear export receptor CRM1 in complex with Snurportin1 and RanGTP. Science *324*, 1087–1091.

Reichmann, D., Cohen, M., Abramovich, R., Dym, O., Lim, D., Strynadka, N.C., and Schreiber, G. (2007). Binding hot spots in the TEM1-BLIP interface in light of its modular architecture. J. Mol. Biol. *365*, 663–679.

Schneider, T.R., and Sheldrick, G.M. (2002). Substructure solution with SHELXD. Acta Crystallogr. D Biol. Crystallogr. *58*, 1772–1779.

Shi, H., and Xu, R.M. (2003). Crystal structure of the Drosophila Mago nashi-Y14 complex. Genes Dev. *17*, 971–976.

Terry, L.J., Shows, E.B., and Wente, S.R. (2007). Crossing the nuclear envelope: hierarchical regulation of nucleocytoplasmic transport. Science *318*, 1412–1416.

Van Duyne, G.D., Standaert, R.F., Karplus, P.A., Schreiber, S.L., and Clardy, J. (1993). Atomic structures of the human immunophilin FKBP-12 complexes with FK506 and rapamycin. J. Mol. Biol. *229*, 105–124.

Vetter, I.R., Arndt, A., Kutay, U., Görlich, D., and Wittinghofer, A. (1999). Structural view of the Ran-Importin beta interaction at 2.3 A resolution. Cell *97*, 635–646.

Weis, K. (2003). Regulating access to the genome: nucleocytoplasmic transport throughout the cell cycle. Cell *112*, 441–451.

Yoshida, K., and Blobel, G. (2001). The karyopherin Kap142p/Msn5p mediates nuclear import and nuclear export of different cargo proteins. J. Cell Biol. *152*, 729–740.

Zhang, Z., and Krainer, A.R. (2007). Splicing remodels messenger ribonucleoprotein architecture via eIF4A3-dependent and -independent recruitment of exon junction complex components. Proc. Natl. Acad. Sci. USA *104*, 11574–11579.